The kinetics of crystallisation of poly(e-caprolactone) measured by FTIR spectroscopy

Phillipson, Kate; Jenkins, Michael; Hay, James

DOI:
10.1007/s10973-015-5047-5

Document Version
Peer reviewed version

Citation for published version (Harvard):
Phillipson, K, Jenkins, M & Hay, J 2016, 'The kinetics of crystallisation of poly(e-caprolactone) measured by FTIR spectroscopy', *Journal of Thermal Analysis and Calorimetry*, vol. 123, no. 2, pp. 1491-1500. https://doi.org/10.1007/s10973-015-5047-5

The kinetics of crystallization of poly (ε-caprolactone) measured by FTIR spectroscopy

Kate Phillipson, Michael J. Jenkins and James N. Hay[1]

The School of Metallurgy and Materials, College of Engineering and Physical Sciences, University of Birmingham, Edgbaston, Birmingham B15 2TT, UK

Abstract.

The kinetics of crystallization of poly (ε-caprolactone), PCL, have been measured by FTIR spectroscopy using the absorbance of the crystalline and amorphous phase carbonyl bands at 1725 and 1735 cm^{-1} respectively to determine the fractional crystallinity as a function of time and over the temperature range 43-47 ^{o}C. A comparison was also made with DSC which was found to have limited sensitivity such that it could only measure the primary stage of the crystallization and not the secondary. Both primary and secondary crystallization could be measured by FTIR spectroscopy with sufficient accuracy to measure the kinetics of each and limited only by the length of time over which the measurements were made.

[1]To whom all communications should be addressed

j.n.hay@bham.ac.uk.

Keywords:

Poly(ε-caprolactone); Isothermal Crystallization Kinetics; Secondary Crystallization; Reptation; Diffusion Control.

1. **Introduction**

Poly (ε-caprolactone), PCL, is a synthetic biodegradable polymer made from the ring opening polymerization of 2-oxepanone. Since it degrades by hydrolysis of the ester groups in physiological conditions it has been used extensively in drug delivery systems and as scaffold material in tissue engineering.

It has a low melting point, about 60 ^{o}C which varies depending on crystallinity and thermal history and has been used as a moulding material since it becomes pliable on immersing in hot water. It is a tough plastic with a very low glass transition temperature at -60 ^{o}C. It ages and embrittles at normal working temperatures such that its material properties are dependent on processing conditions and thermal history. Secondary crystallization is important in establishing the final degree of crystallinity and the distribution of lamellar thicknesses achieved during any thermal treatment. Since it has a pronounced effect on the ultimate material properties achieved it is essential to determine the extent to which material properties are determined by secondary crystallization.

The application of FTIR spectroscopy to measure the development of crystallinity in polyester has recently been reviewed along with the changes in the IR spectra on crystallization, outlining procedures for separating amorphous and crystalline absorption bands [1, 2]. It was observed, by means of two-dimensional correlation spectroscopy, that the carbonyl band at 1720-30 cm^{-1} split into two, at 1725 and 1735 cm^{-1}, attributed to the crystalline and amorphous regions and that the

absorbance of each are inversely related; as one increased the other decreased during crystallization and melting. Unlike DSC, FTIR spectroscopy measured the degree of crystallinity directly and not the rate of change of crystallinity with time such that the overall conversion could be studied over extended time periods well into the secondary process.

This paper investigates the effect of temperature on crystallization kinetics of polymers, both primary and secondary, in more detail than when DSC [3-5] was used and did not have the necessary sensitivity to measure secondary crystallization to any appreciable extent. A comparison is made between the two techniques of FTIR spectroscopy and DSC.

2. Experimental

PCL (CAPA 6800) was supplied in pellet form by Perstorp (Warrington, UK). The number and weight average molecular weights were 80 and 120 kg mol^{-1} respectively, and the polydispersity was 1.5. Films up to 500 μm thick were cast from solution, concentration 3.3-6.6 gdm^{-3}, by evaporation of the solvent, dichloromethane, at room temperature. Traces of solvent were removed by placing the films in a vacuum oven.

Potassium bromide powder, of IR grade, was supplied by Sigma Aldrich (Dorset, UK) and pre-dried in an air-oven overnight at 120 °C before being pressed into discs for IR spectroscopic measurements. Dichloromethane, research grade, was

used as a solvent for PCL. It was supplied by Sigma Aldrich (UK) and used as received.

A Perkin Elmer differential scanning calorimeter, DSC 7, controlled by Pyres software, was used to measure the changes in relative heat flow with time and temperature. A cooling system was attached to the DSC to enable controlled cooling as well as maintain isothermal conditions at room temperature. The temperature scale of the instrument was calibrated from the measured melting points of ultra-pure metals - indium (156.6 °C) and tin (231.9 °C). The power response was calibrated from the enthalpy of fusion of indium, taken to be 28.45 J g^{-1}. Crystallization rate measurements and melting were carried out on film samples encased in aluminium sample pans. Disc shaped samples, cut to size, were placed on top of one another to give approximately 1 mm thick samples with a mass of 16 ± 2 mg. These were sealed with aluminium lids. Samples were heated to 70 °C and held in the melt for 3 min before being cooled, at 320 °C min^{-1}, to the crystallization temperatures. The rate of heat evolved during crystallization was followed as a function of time until the calorimeter response returned to the baseline. The melting behaviour of each sample was also investigated by re-melting each sample after crystallization. The samples were heated from room temperature to 70 °C at a rate of 10 °C min^{-1}.

Transmission FTIR spectra were measured on Nicolet Spectrophotometers, models 1869 and 8700, with DTGS-KBR detector on thin films samples mounted between KBr discs and contained within the furnace of a Linkam hot stage. The

furnace temperature was controlled by a Unicam R600 thermal controller to an accuracy of ± 0.1 ^{o}C. All spectra were recorded at a resolution of 1 cm $^{-1}$ and a total of 400 scans were accumulated for each spectrum. Backgrounds were subtracted from all spectra Pre-dried KBr powder was pressed at a pressure of 15 tons into 16 mm diameter discs, using a Specac, UK die-press. A disc of 300 mg. was used to measure the background. Two sample discs of 150 mg each were produced and used to sandwich the polymer. Drops of polymer solution in dichloromethane were placed on the surface of one of the thin KBr discs and allowed to evaporate. They were subsequently heating in a vacuum oven. The thickness of the sample was adjusted to maintain absorbance values less than 1.0. The polymer film was mounted across the window of the hot stage of a Linkam PR600 hot-stage and placed vertically in the IR beam.

Isothermal crystallization kinetics were measured over the range 40 to 50 ^{o}C, by heating to 70 °C at a rate of 80 °C min^{-1} and held in the melt for 2 min to remove all traces of crystallinity. The sample was cooled to the crystallization temperature and spectra recorded at a resolution of 4 cm^{-1} in sets of 100 scans for 1000 mins

3. Results and Discussion

3.1 Changes to the FTIR Spectrum of PCL on Crystallization

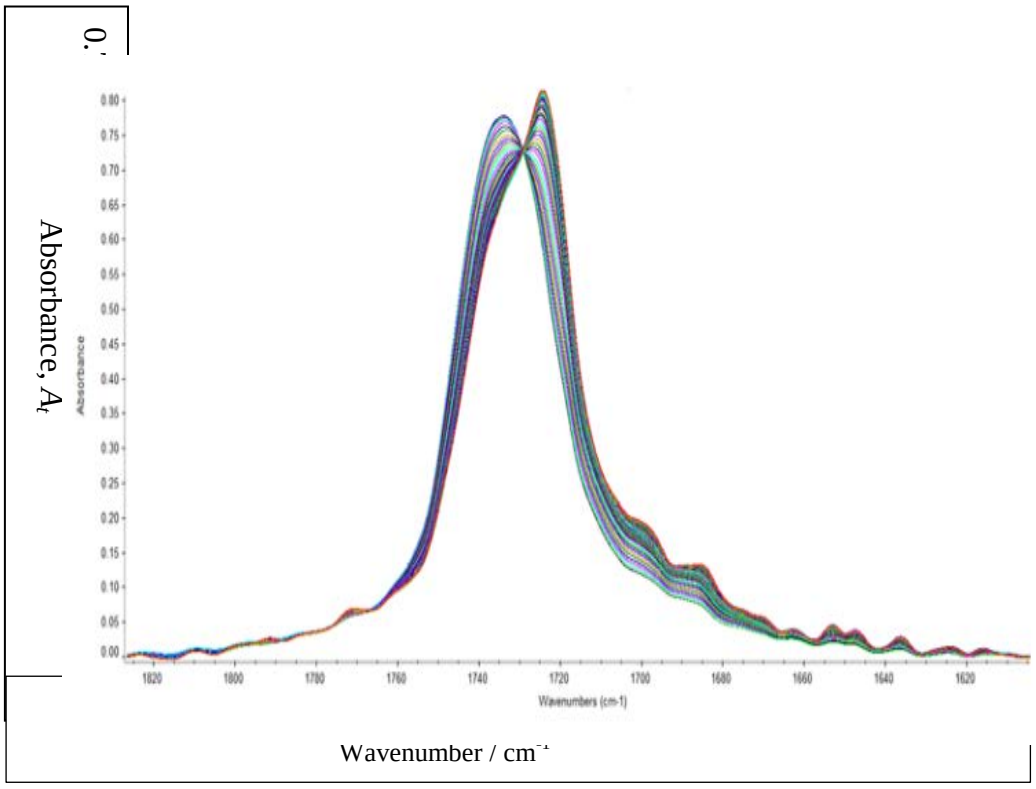

Fig. 1 Change in the carbonyl band at 1730 cm^{-1} on crystallization.

The FTIR spectrum of PCL exhibits the absorption bands of linear aliphatic polyesters with the most intense peak at 1720-30 cm $^{-1}$ characteristic of the stretching of the carbonyl band of the ester group. Marked changes to the shape of this band occur on melting and crystallization. see Fig. 1, which were reproducible on heating and cooling with a decrease in absorption at 1735 and increase at 1725 cm^{-1} with the onset of crystallization.

. The presence of two separate carbonyl bands were attributed to amorphous and crystalline regions respectively and their absorbances used to measure the crystallinity and amorphous fractions by resolving the overlapping carbonyl bands. Base line corrections were applied at two fixed wavenumbers and the absorption band auto-smoothed repeatedly with Omnic software into two absorption bands until the best fit was achieved. The analysis was carried out on the basis of two Laurentzian shaped absorption bands with maximum absorbances at 1735 and 1725 cm^{-1}.

The changes in absorbance of the two bands proceeded simultaneously in that as one increased the other decreased, see Figs. 2 and 3 and the general development of the intensity of the crystalline absorption band with the logarithm of time is shown in Fig. 2 over the isothermal temperature range 43-7 ^{o}C. They have the characteristic dependence on time previously observed in the crystallization of polymers as measured by a range of experimental techniques and attributed to the development of primary and secondary crystallization.

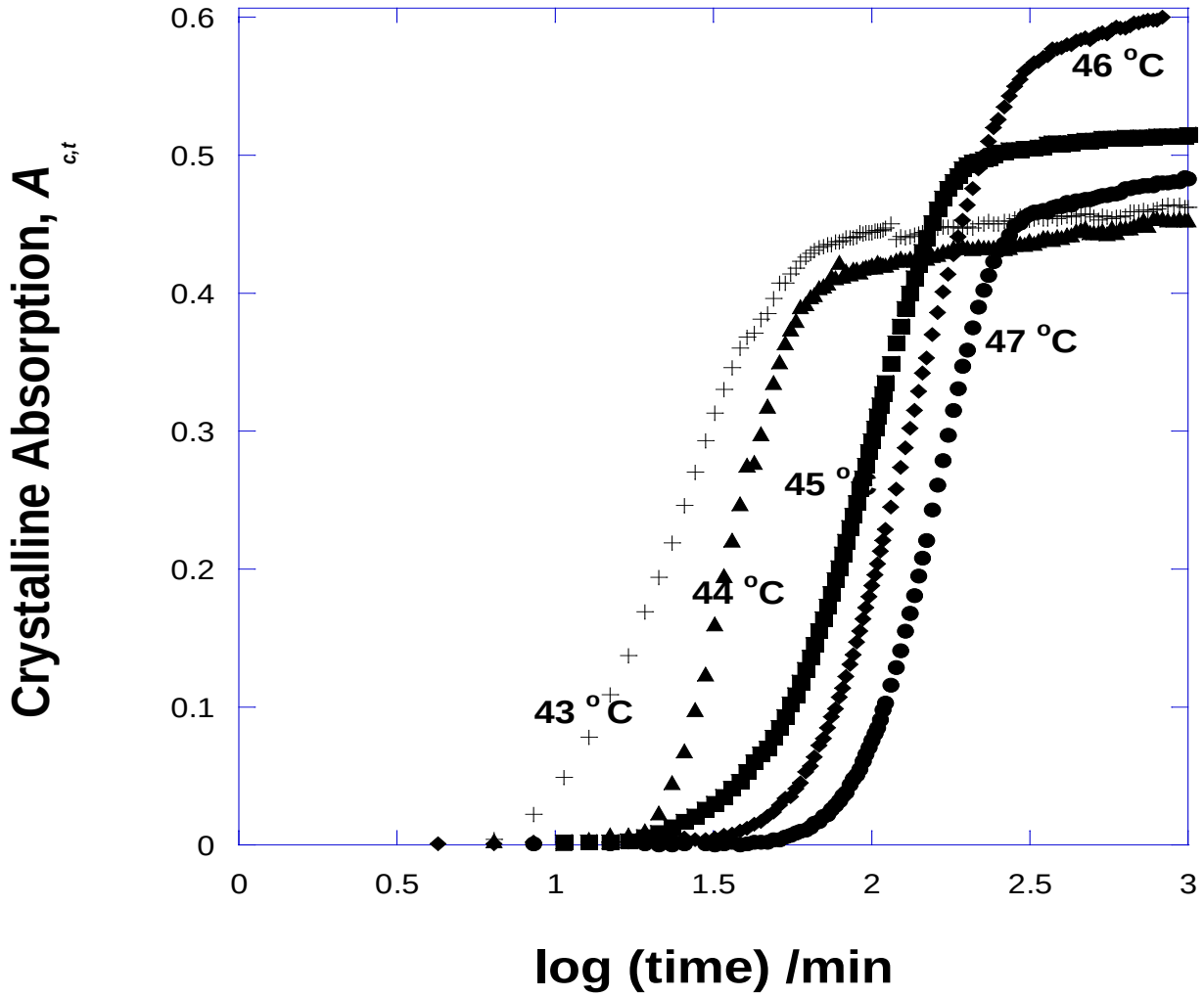

Fig. 2 Increase in crystalline absorption with time.

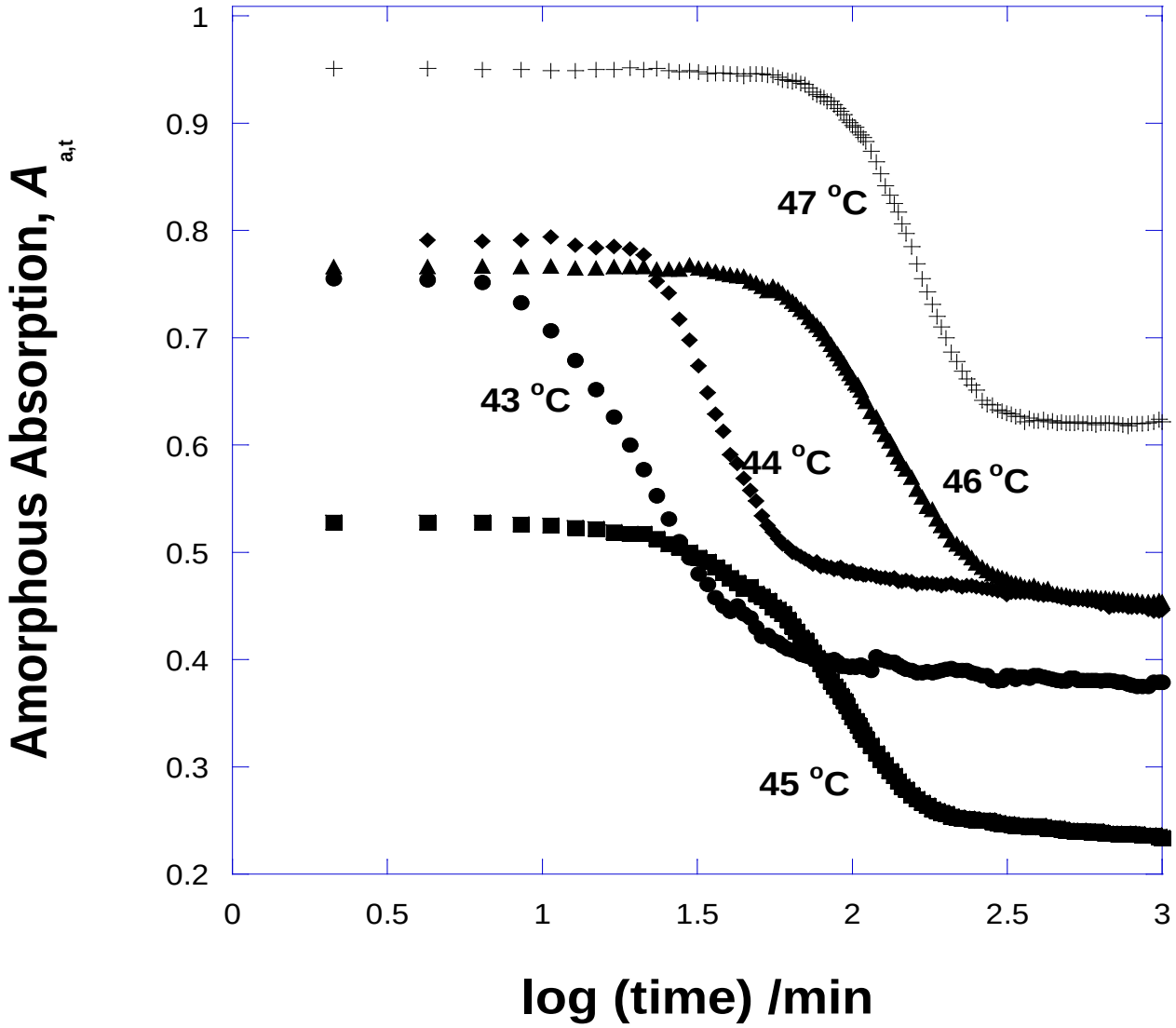

Fig. 3. Decrease in amorphous absorption with time.

The amorphous band exhibited the reverse trend with time, see Fig. 3. Once the isothermal temperature had been achieved there was an apparent induction period during which the absorbance was constant before the absorbance decreased

exponentially as crystallization developed. After this the intensity continued to decrease with time.

3.2. Self-Consistency of the Measurements.

For a two phase model of a partially crystalline polymer, the amorphous weight fraction, $X_{a\,t}$, is related to crystalline weight fraction, $X_{c,\,t,}$ at time t in that

$$X_{a,\,t} + X_{c,\,t} = 1.0 \qquad (1)$$

Defining $X_{a,\,t} = A_{a,\,t}/A_{a,\,o}$

where $A_{a,t}$ and $A_{a,o}$ are the absorbances of the amorphous band at time, *t*, and initially before any crystallinity has developed.

Similarly for the crystalline absorbance,

$$X_{c,\,t} = A_{c,t}/A_{c,\,o.}$$

where $A_{c,t}$ and $A_{c,o}$ are the absorbances of the crystalline band at time, *t*, and the totally crystalline sample,

Since, from eq. 1. $A_{a\,t}/A_{a,o} + A_{c,t}/A_{a,o} = 1,$

then $A_{c,t} = A_{c,o} - A_{a,t}\,(A_{c,o}/A_{a,o)}$ (2).

and $A_{a,t} = A_{a,o} - A_{c,t}\,(A_{a,o}/A_{c,o)}$ (3).

Plots of $A_{c,t}$ against $A_{a,\mathrm{t}}$ and $A_{a,t}$ against $A_{c,t}$ were linear, see Fig. 4, with intercepts of $A_{c,o}$ and $A_{a,o}$. These values were temperature dependent and used to calculate the fractional crystallinity and amorphous content with time at each temperature see Fig 5.

In order to confirm the validity of the analysis the calculated values of the fractional crystallinity, $X_{c,t}$ and amorphous content, $X_{a,t}$, were added together and compared with eq. 1; the addition should be 1.00 for a two phase system and as can be seen from Fig. 6 the average error was better than 0.5%.

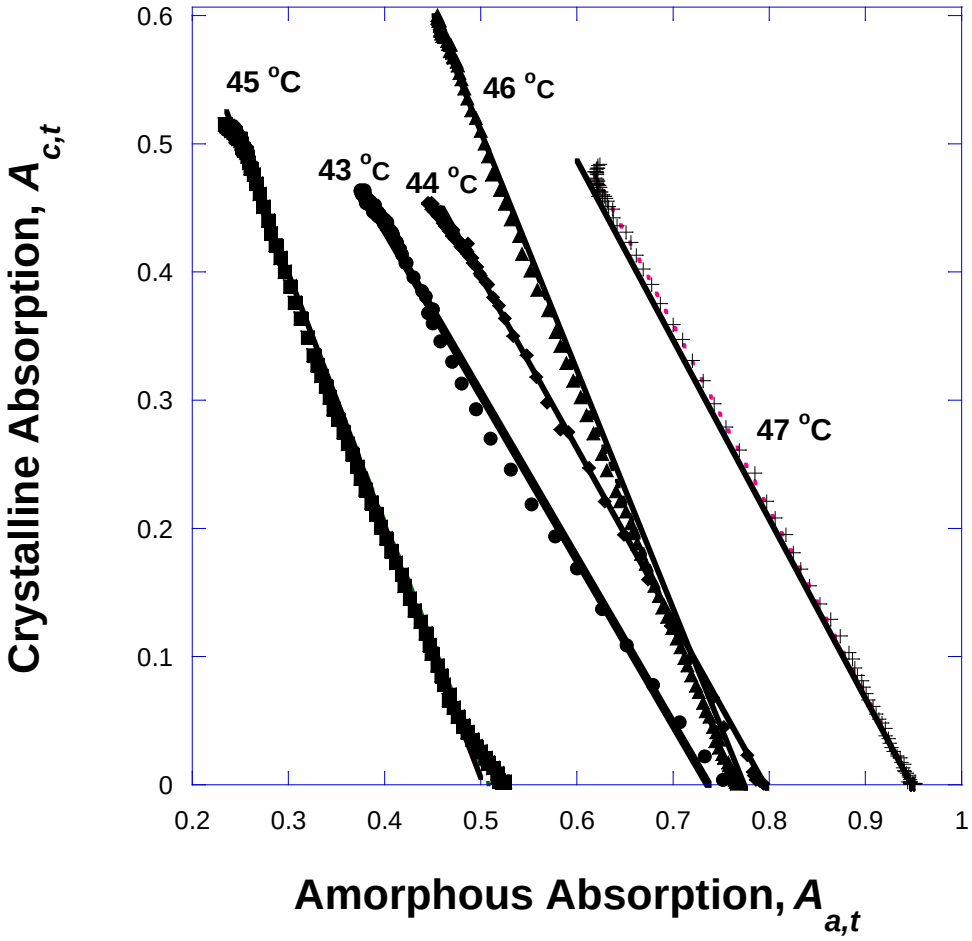

Fig. 4 Dependence of the crystalline on amorphous absorption with crystallization temperature.

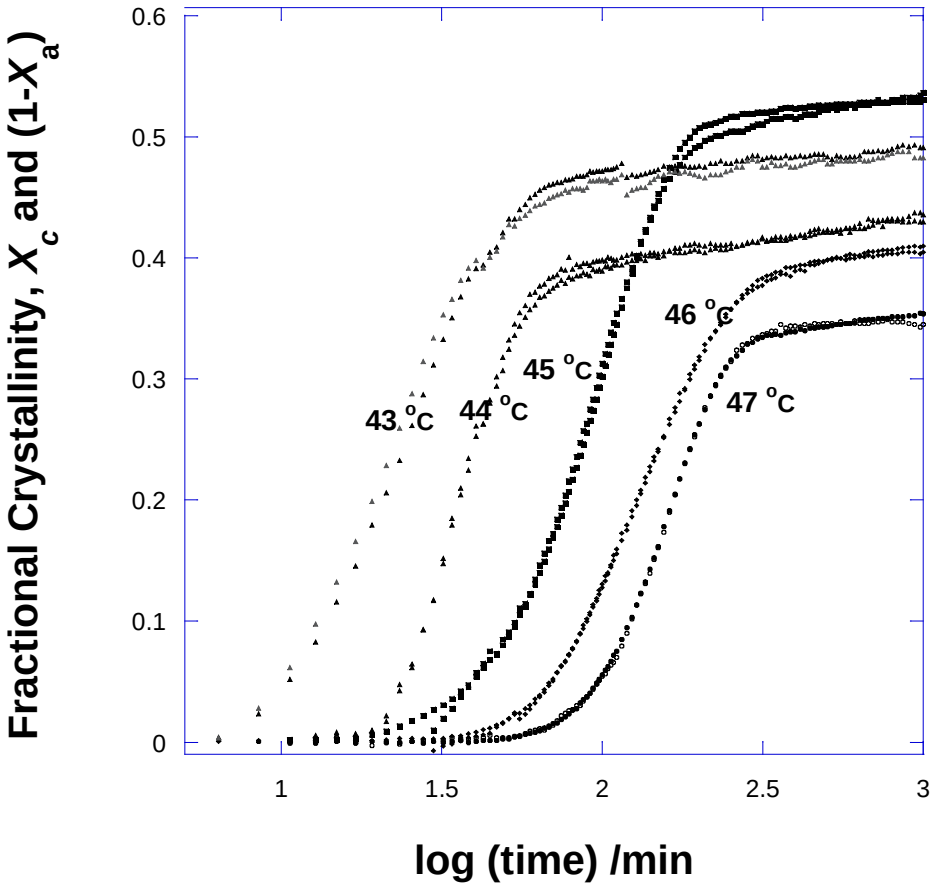

Fig. 5. Comparison of the fractional crystallinity determined from the absorption of the crystalline and amorphous bands .

The fractional crystallinity obtained from the amorphous content, i.e. $(1-X_{a,t})$ was also compared directly with that determined from the crystalline band, $X_{c,t}$, see Fig. 5, at each crystallization temperature. In every case the degree of agreement in

fractional crystallinity between the two sets of data was better than ±0.01. These curves were used to analyze the kinetics of the phase transition.

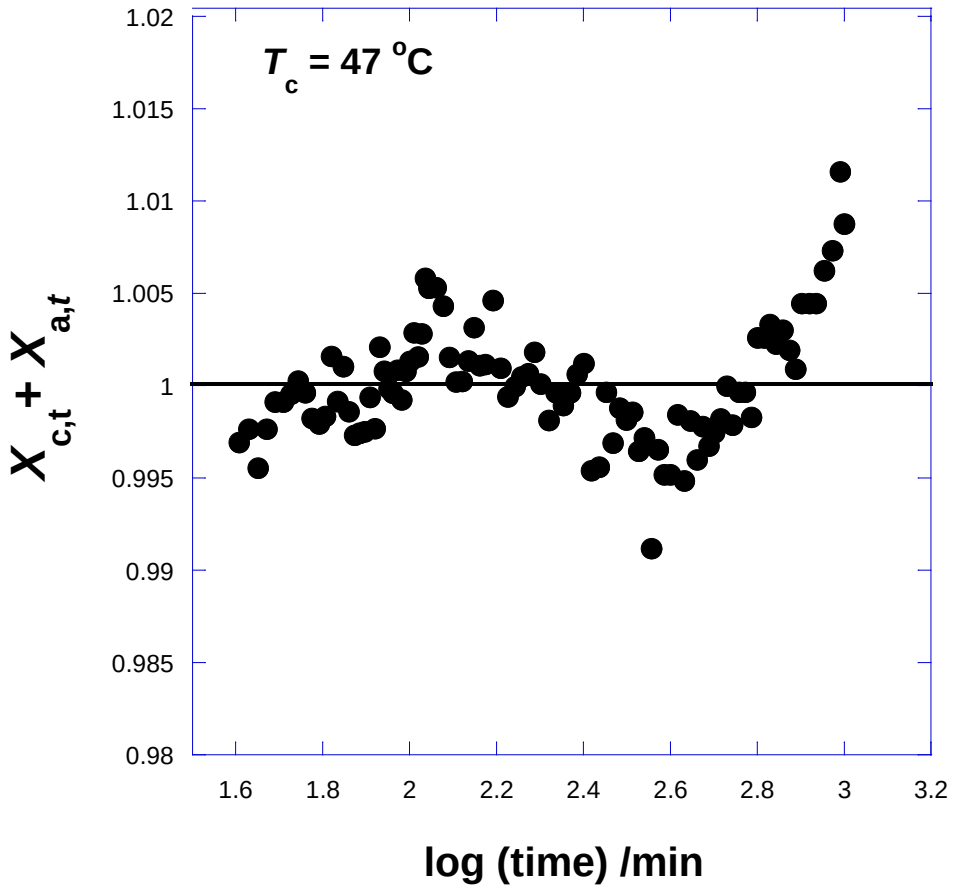

Fig. 6. Consistency of the data with eq. 1 with time.

3.3 Isothermal Crystallization Rate Study

The change in fractional crystallinity as a function of log (*t*) is shown in Fig. 5 over a range of crystallization temperatures, from 43 to 47 °C. Each set is a

combination of X_t and 1-X_a as measured above. They show the displacement of the crystallization to longer times and a decrease in the final degree of crystallinity with increasing temperature.

The initial development of crystallinity appeared to increase following an Avrami equation [6]

i.e. $$1-X_t = \exp(-Zt^n) \quad (4)$$

where X_t is the fractional crystallinity at time *t*, Z a composite rate constant including growth rate and nucleation characteristics, and n a constant whose value depends on the crystallization mechanism.

The final stage of the crystallization was followed by a logarithmic increase with time; conventionally this has been attributed to a secondary crystallization process. In analyzing the data two-stages were adopted, a primary stage in which the crystalline entities grow until they impinged with one another, and a secondary stage in which crystallinity developed further but within the boundaries of the spherulites each following a different time dependence. The primary stage was considered to be limited to a fractional crystallinity, $X_{p,\infty}$, at which the secondary became dominant. The corresponding Avrami equation describing the primary stage was then,

$$X_{p,t} = X_{p,\infty}(1- \exp(-Z_p(t - t_i)^n) \quad (5)$$

where $X_{p,t}$, Z_p and n are the fractional crystallinity developed at time *t* in the primary stage, a composite rate constant and exponent of the primary process. The induction time, t_i and fractional crystallinity at the end of the primary process $X_{p,\infty}$ were treated

as adjustable parameters and selected to represent the initial onset and the end of the primary process

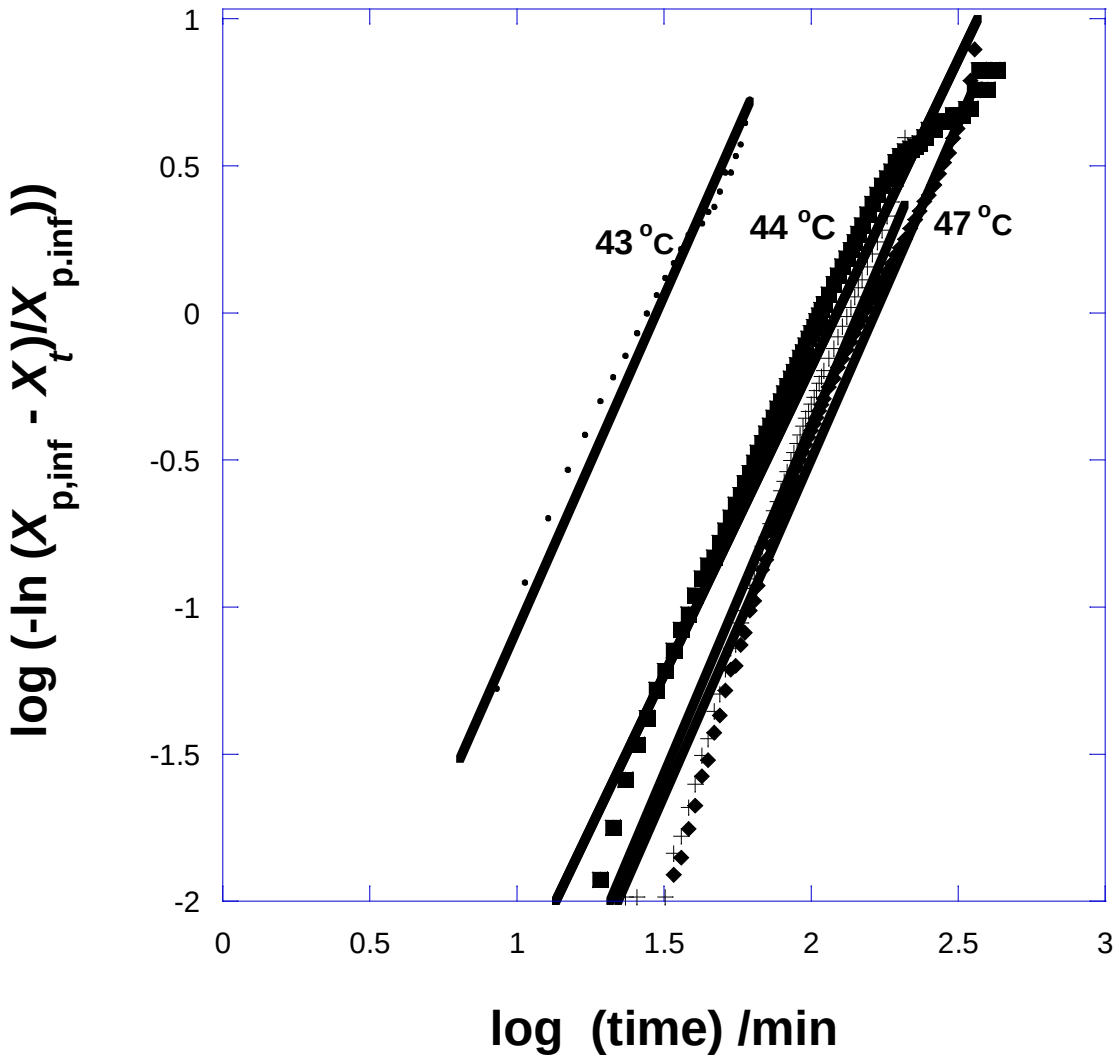

Fig. 7. Analysis of the primary process.

T_i = 0 min.

Optimum values of $X_{p.inf}$ were selected from the intersection of the primary and secondary processes. From equation (5)

$$\log(-\ln(X_{p,\infty} - X_{p.t})) = n \log(t - t_i) + \log(Z_p) \quad (6)$$

n values and rate constants, Z_p , see Table 1, were determined from the slopes and intercepts at t= 1 of the linear plots of $\log[-\ln(1-X_{p,t}/X_{p,\infty})]$ against $\log(t)$. The optimum fit of the experimental data is shown for each temperature in Fig. 7.

Table 1. Primary Crystallization Avrami Constants

Crystallization Temperature / ^{o}C	Fractional Crystallinity $X_{p,\infty}$	n Value ± 0.2	Induction Time / min	Half Life $t_{1/2/}$ min	Rate Constant Z_p / min^{-n} x 10^8
43.0	0.455	2.36	0	20	8150
44.0	0.395	3.12	5	30	171
45.0	0.500	2.61	10	74	10.2
46.0	0.390	2.30	15	108	14.6
47.0	0.330	2.61	20	130	1.91

Fig. 8 show the effect of varying the induction time, t_i, on the linearity of the log (ln)-log plots and the sums of the squares of the residuals, R^2, was used to determine the optimum values of t_i for each temperature and this in turn the value of n corresponding to a maximum in R^2, see Fig 9. Crystallization rate parameters for the

primary process determined in this way are listed in Table 1. The half-lives, $t_{1/2}$, were taken to be the time corresponding to $X_{p,t} = X_{p,\infty}/2$. The composite rate constant decreased with increasing temperature which is characteristic of nucleation control of the crystallization and the dependence of rate on the degree of supercooling. From the best fit values of $X_{p,\infty}$ it can be seen that the primary process was restricted to the first 35-50 % crystallinity and this decreased with crystallization temperature.

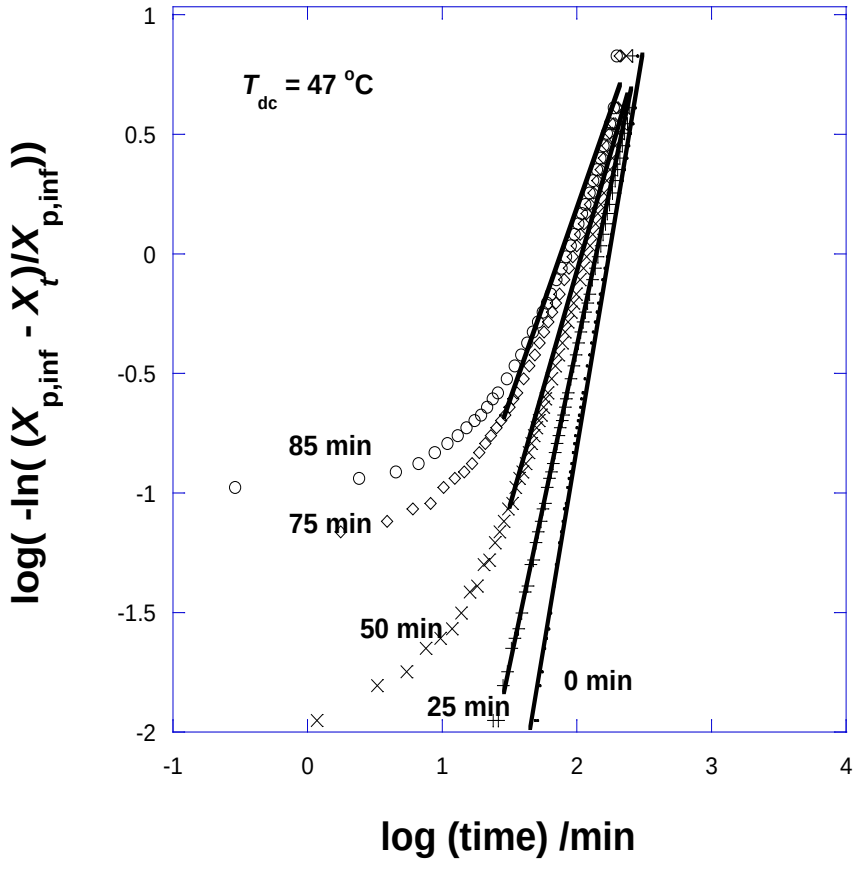

Figure 8. The effect of induction time on the linearity of the (log (-ln($X_{p,inf}$ - X_t)/$X_{p,inf}$)) plots.

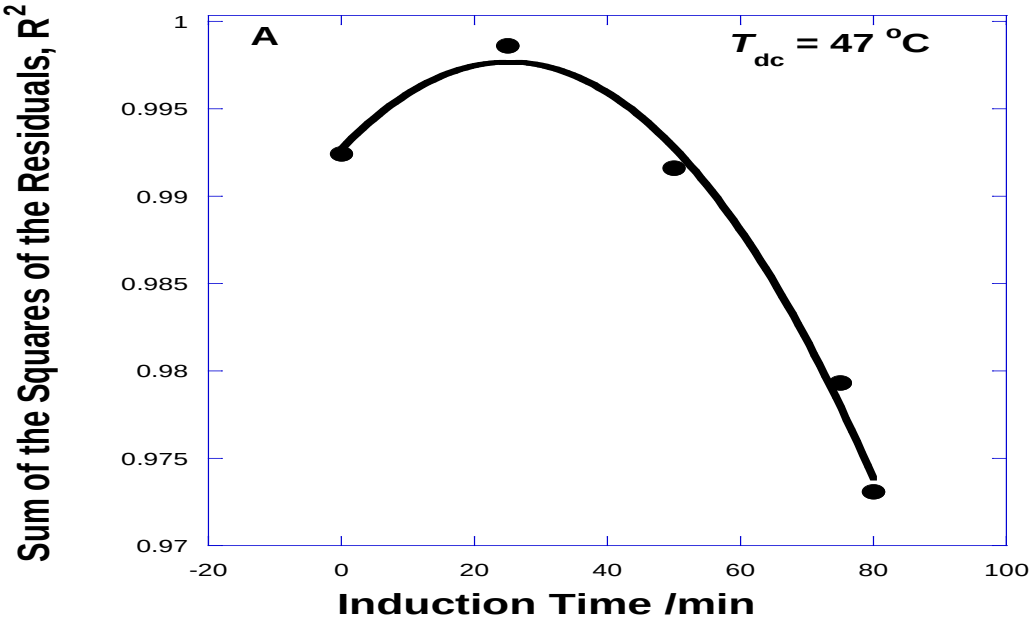

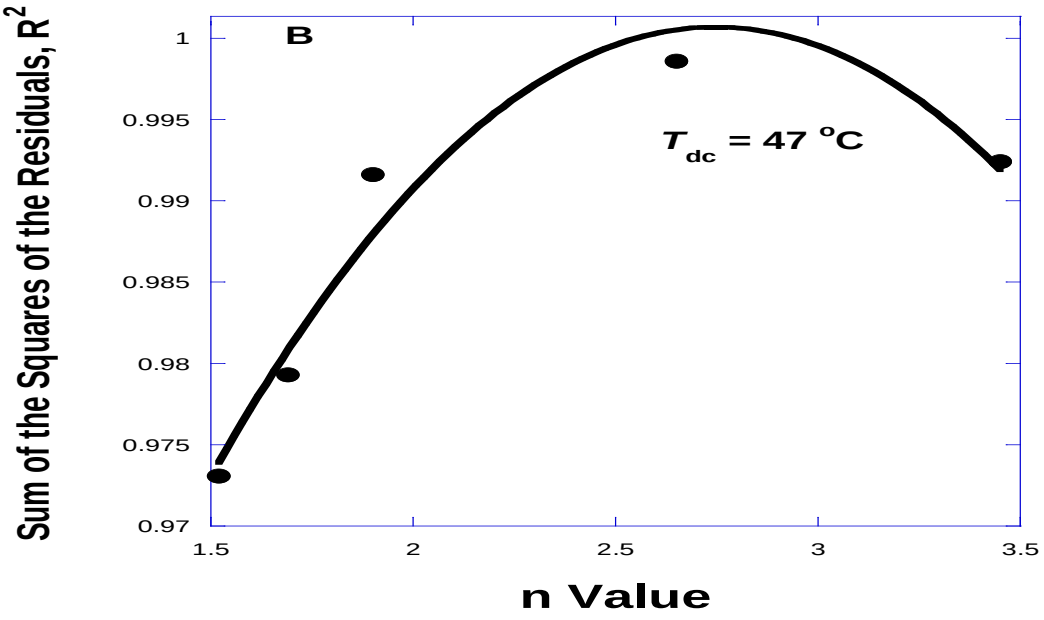

B.

Fig. 9. Effect of Induction time on

A) degree of fit and B) n value.

Fractional n values between 2.3 and 3.1 ± 0.2 were observed which have in the past been interpreted as predetermined nucleation of spherulites and is in reasonable agreement with the Avrami model which should produce an n value of 3.0. Although the n values were fractional they were close to the expected integer value of 3.0 for this crystallization model as discussed by Avrami [6]. There are many reasons cited in the literature, such as non-uniform nucleation and non-negligible volume of nuclei for non-integer values of n [7].

3.4. DSC Crystallization Rate Studies.

The crystallization of PCL was also measured by DSC for comparison with the FTIR spectroscopic study. The DSC thermal response during crystallization is shown in Fig. 10 but since the DSC was less sensitive to measuring changes in crystallinity than FTIR spectroscopy the measurements were confined to faster rates and lower temperatures, 38 to 42 ^{o}C. This restricted the rate studies to very much shorter times; 60 min. rather than 1000 min. before the calorimeter response returned to the baseline.

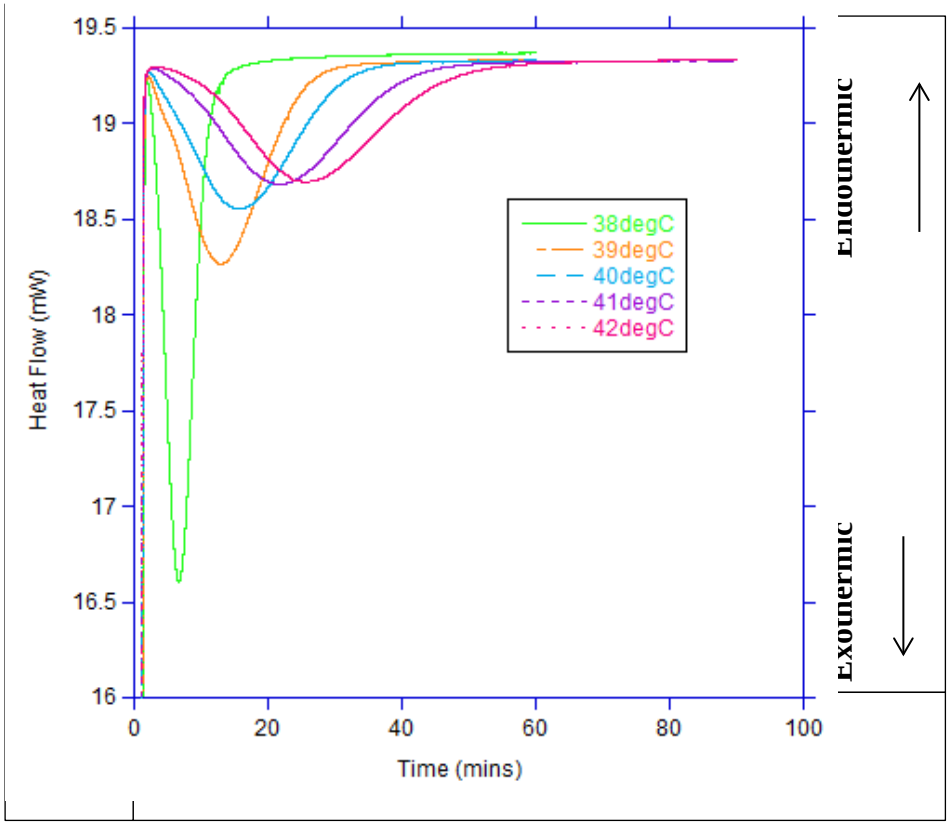

Fig. 10 – Change in heat flow (exothermic down) with time on crystallizing at 38-42 °C.

The relative crystallinity, X_t, was calculated as a function of time at each isothermal temperature from the fractional increase in area with time, i.e.

$$X_t = \int_0^t (\mathrm{d}H/\mathrm{d}t).\mathrm{d}t / \int_0^\infty (\mathrm{d}H/\mathrm{d}t).\mathrm{d}t \qquad (7).$$

where dH/dt is the heat flow rate at time t. The relative crystallinity followed an exponential increase with time consistent with the primary process observed by FTIR spectroscopy but was not followed by any dependence on log time attributed to secondary crystallization, see Fig. 11.

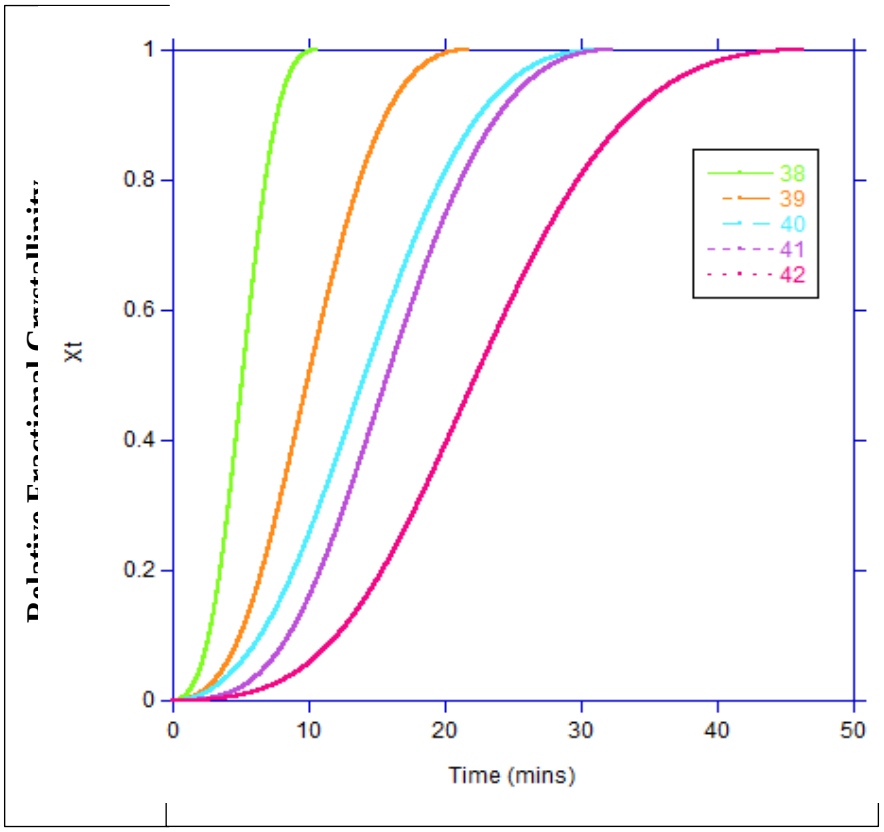

Fig. 11. – Growth of relative fractional crystallinity, X_t, with time on crystallising at 38-42 °C.

The relative crystallinity dependence on time was time analyzed as before by the Avrami equation to determine the composite rate constant Z_p and the value of n. From equation (6) plots of log [-ln(1-*X*t)] against log(*t*) were linear with a slope of n and an intercept at log(*t*) = 0 of log (Z_p); the result of this analysis is shown in Table 2. The n values varied between 2.5 and 3.0 and were consistent with those observed previously in the analysis of the primary process using FTIR spectroscopy.

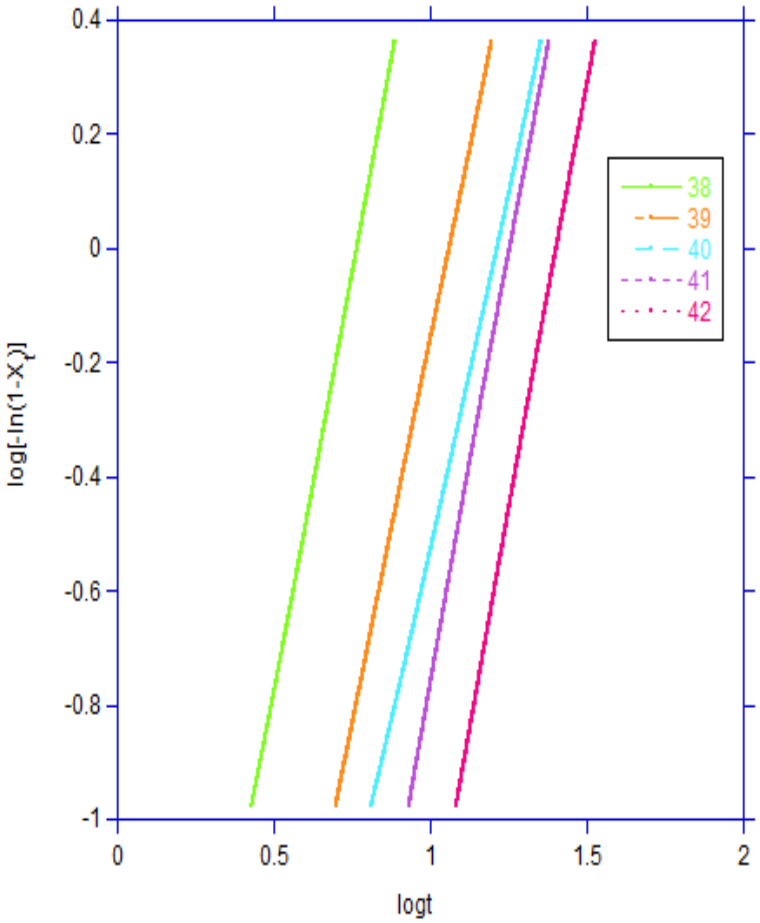

Fig. 12 – Analysis of crystallization time dependence. Isothermal crystallisation at 38-42 °C.

Table 2. DSC Rate Parameters.

Crystallization Temperature / ^{o} C	n Value ± 0.1	Half Life $t_{1/2}$ / min	Composite Rate Constant Z_p/ min x 10^3	Relative $X_{p,\infty}$
38.0	2.9	5.0	6.51	0.95
39.0	2.5	10.0	2.19	0.90
40.0	2.6	13.3	0.830	0.90
41.0	2.9	17.5	0.172	0.90
42.0	3.1	22.5	0.042	0.90

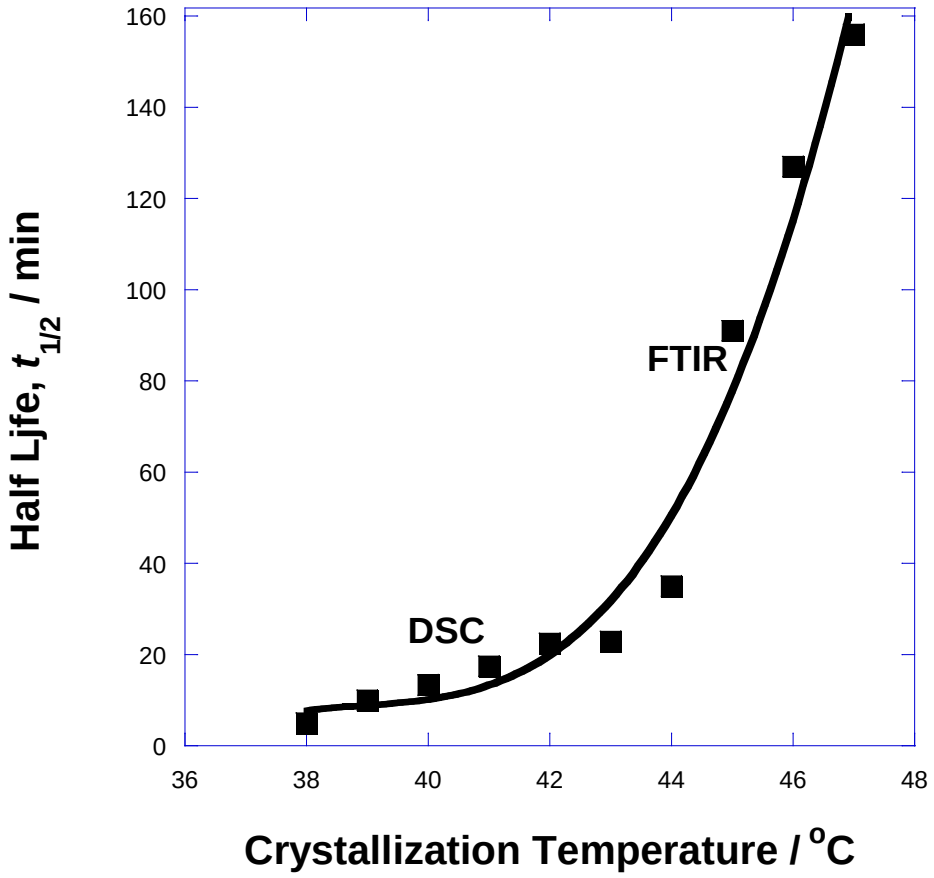

Fig. 13. A comparison of the half-lives of primary crystallization measured by DSC (38-42 °C) and FTIR spectroscopy (43 -47 °C)

The crystallization half-life, $t_{1/2}$, at each temperature was read directly from Fig. 10 as the time corresponding to $X_t = X_{p,\infty}/2$. The half-lives increased steadily with increasing crystallization temperature consistent with nucleation control of the crystallization and a slowing down of the rate as the melting point is approached and the values were consistent with the half-lives of the primary process as measured by

FTIR spectroscopy, see Fig. 13 where the two sets of data are compared directly, indicating that both techniques are measuring the primary stage of the crystallization.

3.5 Secondary Crystallization.

Several kinetic equations have been derived to follow the development of secondary crystallization with time. Most authors consider that it obeys an Avrami equation with n=1.0 due to a 1- dimension increase in thickness of the lamellae with impingement on adjacent lamellae. However, this suggests a dependence of log (X_t) on time and cannot account for the observe dependence of X_t on log time. It also gives a poor fit of the crystallization –time data [8, 9]. Recently we have observed that secondary crystallization of PET [10,11] is associated with an increase in lamellae thickness and local diffusion of the chain segments on to the growth face for which the secondary crystallinity, $X_{s,t}$, increases with the square root of the crystallization time. If it is assumed that secondary crystallization occurs within the boundaries of the spherulites, and develops with the extent of primary crystallization, $X_{p,t}$, then

$$X_t = X_{p,t} + X_{s,t} = X_{p,t} + X_{p,t} k_s t^{½}$$

$$= X_{p,\infty} (1\text{-}\exp\text{-}Z_p t^n) (1+ k_s t^{1/2}) \quad (8)$$

At values of $X_t > X_{p,\infty}$, the primary process has stopped and the function

$$\exp(-Z_p t^n) = 0 \quad (9)$$

The increase in fractional crystallinity with time becomes,

$$X_{s,t} = X_{p,\infty} (1+ k_s t^{1/2}) \qquad (10)$$

$X_{s,,t}$ was analyzed after the primary process had terminated and a linear plot of $X_{s,t}$ against $t^{1/2}$ was observed from which k_s was determined, see Fig. 14 and Table 3. The uncertainty in k_s listed arises from the error in determining X_c (±0.005) and the small increment in X_c over the whole secondary process (0.02-0.05). Nevertheless there is an increase in diffusion rate with temperature consistent with it being a thermally activated process obeying Arrhenius dependence i.e. $k_s = A, \exp(- \Delta E/RT)$

where A is pre-exponential factor, ΔE the activation energy for diffusion, R gas constant and T temperature. The activation energy over this limited temperature range was determined to be about 40±10 kJ mol^{-1}.

Table 3. Diffusion Coefficient for Secondary Crystallization.

Crystallization Temperature / ^{o}C	Fractional Crystallinity $X_{p,\infty}$	Diffusion rate k_s x 10^{3} / $min^{-1/2}$
43	0.49 ± 0.01	1.92 ± 0.5
44	0.40 ± 0.01	4.25 ± 2.0
45	0.52 ± 0.01	1.00 ± 0.5
46	0.40 ± 0.01	3.39 ± 1.0
47	0.34 ± 0.01	3.72 ± 1.0

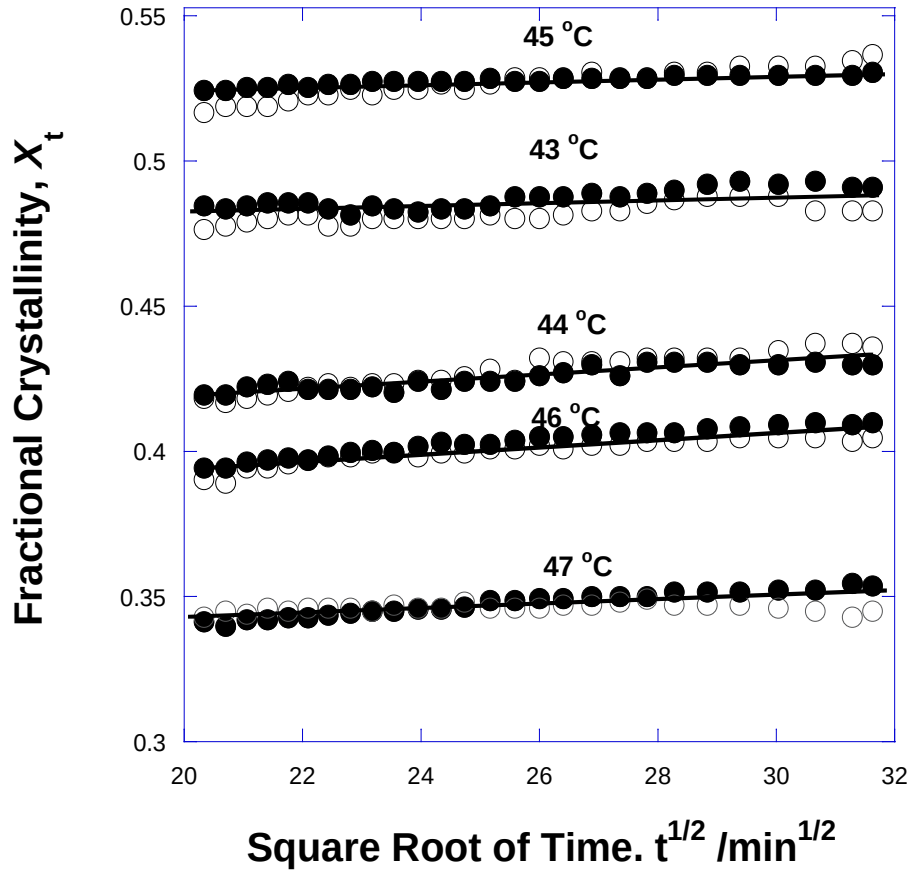

Fig. 14. The increase in fractional crystallinity due to secondary crystallization with the square root of the crystallization time.

● X_c ○ 1-X_a

3.6 The Temperature Dependence of Primary Crystallization.

The primary crystallization rates at different temperatures were expressed in the form of reciprocal crystallization half-life, $1/t_{1/2}$, using the Hoffman-Lauritzen relationship [12]. Since the half-lives were determined directly from the X_t v t data they were independent of the analytical procedure adopted. $(1/t_{1/2})$ values were substituted for the crystal growth rates, g and g_0, respectively [13] and the dependence of the crystallization half-life given by,

$$(1/t_{1/2}) = (1/t_{1/2,0}) \exp(-U^*/R(T-T_2).\exp(-K/T_c(\Delta T)) \qquad (12)$$

where U^* is the activation energy of viscous flow and taken to be 6284 J mol.$^{-1}$ [14], T_2 is the thermodynamic glass transition temperature, K the nucleation constant, T_c the crystallization temperature, and ΔT the super-cooling from the equilibrium melting point, T^o_m. Plots of ln $(1/t_{1/2})+U^*/R(T-T_2))$ against $1/(T\Delta T)$ were linear, see Fig. 15, with a slope of $1.8x10^5$ K^2, corresponding to the nucleation regime I.

Regime I is considered to occur at high crystallization temperatures and low degree of super-cooling in which secondary nucleation is rate determining, coverage of the crystal growth face with new material occurs rapidly compared with nucleation and there is a delay before the next layer is nucleated. For this model, [13] the growing surface is smooth, and

$$K_1 = 4\, b\sigma\sigma_e T^o_m / k\Delta H_V \qquad (13)$$

where b is the monomolecular layer thickness, taken to be the perpendicular separation of (010) planes, σ is the side surface free energy of the polymer crystal, σ_e

the fold surface free energy, k is Boltzmann constant and ΔH_v the enthalpy of fusion per unit volume. T^o_m the equilibrium melting point of PCL was taken to be 352.2 K

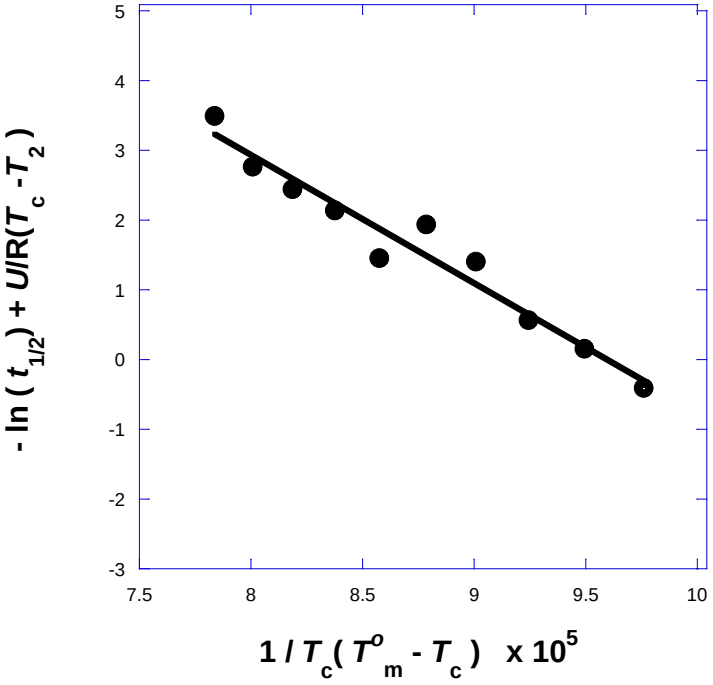

Fig. 15. Dependence of the half-lives of primary crystallization on the degree of super-cooling.

Using the crystallographic unit cell dimensions of a= 7.496 x 10^{-10} m, b = 4.974 x 10^{-10} m and c = 17.277 x 10^{-10} m and with 4 monomer units per unit cell [14], the heat of fusion per unit volume, $\Delta H_{v,}$ was calculated to be 118.7 J cm^{-3} and the crystalline density, 1.174 g cm^{-3}. σ was estimated from [4, 12, 15]

$$\sigma = 0.11 \Delta H_v (ab)^{1/2} \qquad (14)$$

Accordingly σ was 7.97x10^{-3} and σ_e 5.49x10^{-2} Jcm^{-2}, which compared well with the values determined for PET [2].

4.0 Conclusions.

Two different crystallization mechanisms have been observed in the crystallization of PCL which are associated with primary and secondary crystallization. From this and previous work [2, 10, 11] these are considered to be universally applicable to the melt crystallization of polymers.

The primary and secondary stages are readily distinguished by their different time dependences. The primary develops by nucleation and growth of branching lamellae which develop into spheres and grow linearly with time. An Avrami equation with n= 3.0 readily accounts for the exponential increase in fractional crystallinity with time and with the observed linear growth. The temperature dependence of growth and the thickness of the lamellae are nucleation control and can be accounted for by the theory of Hoffman and Weekes [15] The lamellae grow by secondary nucleation of the lateral face in Regime 1 and the nucleation is rate determining. Since this is followed by rapid coverage of the nucleated surface, the growth face is molecularly smooth and the lamellae thickness is constant at a critical value determined by the degree of supercooling.

A different mechanism is required to explain the very low time dependence of the secondary process, the change in melting point and lamellar thickening with the extent of secondary crystallization, the linear dependence of the increase in crystallinity with the square root of time, and the increase in rate with temperature.

These observations are inconsistent with nucleation but consistent with diffusion control.

De Gennes [16] and later Doi and Edwards [17] have pointed out that the long ranged mobility of polymer chains in a polymer melt are highly restricted by entanglements between adjacent chains. The chain segments of an individual chain are so restricting that long range displacement greater than the separation between adjacent entanglements can only occur by reptation of the chain segments. They envisaged that each chain exist in a virtual tube created by the presence of adjacent chains which are excluded from it. An individual chain could only move by segments rotating backwards and forwards within the tube - a process of reptation. The tube is not formed by van der Waals forces creating an excluded volume but by the presence of the entanglements between adjacent chains such that the diameter of the tube is of the order of the distance between adjacent entanglements along a chain. The diameter of the tube is of the order of several microns. It is considered that the tube forms and reforms immediately an entanglement disappears and it also follows the contour of the chain as it diffuses through the melt. This theory has been successful in accounting for the melt viscosity of a polymer melt and partly its dependence on the molecular weight of a polymer above the onset of entanglements, i.e. $M^{3.4}$.

Two diffusion mechanisms and the time dependence of segmental mobility are important in the Reptation Theory [17] and have been observed in self diffusion studies using deuterated polymers [18, 19] and computer modelling of polymer chains

diffusing [20]; these are a dependence of diffusion distance on time, i.e. t and on the square root of time, i.e. $t^{1/2}$. In diffusion over distances greater than the tube diameter the displacement of the segments is constrained by entanglements and the process is that of large number of segments reptating. For this, the displacement over time, t ,

$$<(Rn(t) - Rn(0)> = k' t \qquad (18)$$

Incorporating the reptation theory of the melt mobility into Hoffman and Weekes model of nucleation of lamellar crystals primary crystallization occurs by the lateral extension in the ab direction of the unit cell and involves the sufficient segments of the chain to cover the full stem length. This is many times greater than the number of segments between entanglements in the melt and the reeling in of the chain segments on to the growth face will be inhibited by entanglements. Diffusion of this length of chain will follow eq. 17 and a linear dependence of the growth rate on time will be observed. The average lamellae stem length is many times the radius of the virtual tube, about 10 to 100 nm cf.3-5 nm. Diffusion of the segments on to the critical size nuclei and subsequent growth will be constrained by chain entanglements and growth will be linear with time. The growth, however, is nucleation controlled and this is the rate determining step.

If however, the segmental displacement is less than the distance between adjacent entanglements then the segments involve is not constrained by the entanglements and the displacement of chain segments is

$$<(Rn(t) - Rn(0)> = k t^{1/2} \qquad (17).$$

Where k' and k are the corresponding diffusion coefficients. If as has been suggested lamellae thickening occurs at edge and step dislocations [21] the reduced surface energy contribution to the energy of formation of the nucleus will decrease the critical thickness of the tertiary nuclei to below the entanglement distance and growth will increase along the thickness of the lamellae with the square root of time and nucleation ceases to be the rate determining step.

To conclude, secondary crystallization occurs by extension of the "fold surface" and the thickening of the lamellae. The time dependence of growth can only be explained by small segments of the chain being incorporated on to the crystal on the time scale of the local segmental mobility and independent of entanglements. This does not have the characteristics of a nucleation controlled process but increases in rate with increasing temperature, Since it has been observed [21] that the thickness of lamellae at a fixed radius within a spherulite is constant and decreases as the radius increases secondary crystallization must develop as soon as the lamella develops from the melt and continue to develop with the square root of the lapsed time . This is also consistent with melting being observed to start from the boundary of the spherulites where the thinnest lamellae are present.

5. Acknowledgments

We would like to thank Mr. Frank Biddlestone for technical support.

6. References

[1] Chen Z, Hay JN, Jenkins MJ. Eur Poly J, 2012; **48**: 1586-1610.

[2] Chen Z, Hay JN, Jenkins MJ. Eur Poly J, 2013; **49**:1722

[3] Henricks J, Boyum M, Zheng. J. Therm. Anal. Calorm. 2015; 120: 1765-74.

[4]. Liu G. J. Therm Anal. Calorm. 2014; 114: 1401-6.

[5] Schawe JEK, . J. Therm Anal. Calorm. 2014; 116: 1165-74.

[6] Avrami MJ, J Chem Phys, 1939; 7: 1103-12.

[7] Cheng SZD, Wunderlich B, Macromolecules, 1988 ;**21** :3327-8.

[8] Hillier IH, J Poly Sci, A,1965; **3** :3067-78..

[9] Hay JN, Booth A, Brit Poly J, 1972; **4**: 19-26.

[10] Chen Z, Hay JN, Jenkins MJ, Eur Poly J, 2013; **49:** 2697-703.

[11] Chen Z, Hay JN, Jenkins MJ, Eur Poly J, 2014; **50**:235-447.

[12] Hoffman JD, Weekes JJ, J Chem Phys, 1962; **37**:1723-39.

[13] Chan TW, Isayev AI, Polym Eng Sci, 1994; **34**: 461-71.

[14] Bittiger H, Marchessault RH, and Niegisch W D, Act Cryst., 1970, **B26**, 1923-27.

[15] Hoffman JD, Frolen LJ, Ross, GS, Lauritzen, J. I. jr., J Res NBS, 1975; 79A (6): 671-700.

[16] De Gennes PG, J Chem Phys 1971; 55: 572-9.

[17] Edwards SF, and Doi M, The Theory of Polymer Dynamics, Oxford University Press, Oxford 1988; J Chem Soc, Faraday Trans 2, 1978;**74**: 17891901.

[18] Kim K, Sperling LH, Klein A, Hammouda B, Macromolecules, 1994;27: 6841-50.

[19] Klein J, Briscoe BJ, Proc Roy Soc, London 1979 ; A**365**:53-73.

[[20] Baumgartner A, Ebert U, Schafer l, J Statistical Phys, 1998; **90:**1376-400.

[21] Abo el Maaty, MI, Bassett, DC, Polymer,2005; **46**: 8682-8.